*J. Fluid Mech.* (1990), *vol.* 220, *pp.* 595–621
*Printed in Great Britain*



# The evolution of a localized disturbance in a laminar boundary layer. Part 2. Strong disturbances

By KENNETH S. BREUER† AND MARTEN T. LANDAHL
Department of Aeronautics and Astronautics, Massachusetts Institute of Technology, Cambridge, MA 02139, USA

(Received 31 August 1989 and in revised form 5 April 1990)

Navier–Stokes calculations were performed to simulate the evolution of a moderate-amplitude localized disturbance in a laminar flat-plate boundary layer. It was found that, in accordance with previous results for linear and weakly nonlinear disturbances, the evolving disturbance consists of two parts: an advective, or transient portion which travels at approximately the local mean velocity, and a dispersive wave portion which grows or decays according to Tollmien–Schlichting instability theory. The advective portion grows much more rapidly than the wave portion, initially linearly in time and, in contrast to the weak-disturbance case, gives rise to two distinct nonlinear effects. The first is a streamwise growth of the disturbed region producing a low-speed streak, bounded in the vertical and spanwise directions by intense shear layers. The second nonlinear effect is the onset of a secondary instability on the vertical shear layer formed as a result of spanwise stretching of the mean vorticity and giving rise to oscillations in the $v$- and $w$-components with a substantially smaller spatial scale than that of the initial disturbance. The effect of initial spanwise scale is assessed by calculating the disturbance for three different cases in which the spanwise scale and the initial disturbance amplitude were varied. It was found that the resulting perturbation depends primarily on the initial distribution of $v$ in each plane $z = \text{const.}$, but is approximately independent of the spanwise scale.

## 1. Introduction

Transition to turbulence has been intensely studied over the past few decades and much progress has been made in the understanding of linear and nonlinear processes in the instability and breakdown of wall-bounded shear flows. While the majority of research has focused on the evolution of initially two-dimensional infinite wave trains, there has recently been some interest in the evolution of localized disturbances in a laminar flow. Case (1960) showed that a two-dimensional inviscid disturbance may be characterized as being composed of two parts: a 'wave' part and a 'transient' or 'advective' part. The wave portion is the part of the disturbance that is usually considered in stability theory and is composed of the dispersive waves travelling with a characteristic velocity and growth rate which are found as eigenvalues of the Rayleigh equation. In contrast, the transient part of the disturbance travels at the local mean velocity of the fluid and, as Gustavsson (1978) showed, decays as $1/t$ for a two-dimensional flow.

† Present address: Center for Fluid Mechanics, Turbulence and Computation, Box 1966, Brown University, Providence, RI 02912, USA.

For a three-dimensional flow, the transient portion has a very different character. This was recognized by Landahl (1975), who noted that for an initial disturbance with a spanwise structure, the transient part of the solution contains a non-vanishing component, which he termed the 'liftup' effect, in which the integrated effect of the vertical perturbations creates large-amplitude, non-vanishing, perturbations in the horizontal velocities through the generation of vertical vorticity, and the tilting and stretching of vortex lines. The role of vortex tilting and stretching has long been recognized in connection with three-dimensional secondary instabilities of Tollmien–Schlichting waves (see, for example, Kovasznay, Komoda & Vasudeva 1962; Stuart 1965; Wray & Hussaini 1984; Orszag & Patera 1983), and the application of these ideas to localized disturbances has been reported by Gustavsson (1978), Henningson (1988) and by Breuer & Haritonidis (1990) in Part 1 of this work (hereinafter referred to as Part 1). These studies have shown that, for an inviscid flow, the transient part of the three-dimensional disturbance grows owing to the generation of vertical vorticity by the liftup effect, forming an inclined shear layer which is tilted and stretched by the mean shear as it travels downstream. This growth occurs even though all of the free wave modes of the inviscid disturbance are damped. Landahl (1980) has also shown that for a linear inviscid flow, a three-dimensional initial disturbance is subject to an algebraic instability by which the disturbance energy grows at least as fast as linearly with time owing to the elongation of the disturbance's structure.

The inclusion of small viscosity does not significantly change the short-time evolution of the disturbance. Experimental results presented in Part 1 show that for a low-amplitude initial perturbation, the disturbance initially behaves as the inviscid theory predicts, forming a shear layer which is tilted and stretched by the action of the mean shear as it advects downstream. However, at the Reynolds number and amplitude that were considered in Part 1, the transient part of the disturbance eventually decayed (as viscous linear theory dictates), leaving only the dispersive portion of the disturbance in the form of a linearly unstable wave packet which grew slowly as it travelled downstream, in accordance with the linear stability theory. A weak nonlinearity was also observed by comparing disturbances of opposite phase, but this nonlinearity also decayed and did not affect the resultant wave packet. The growth and evolution of such wave packets has been studied in detail by Gaster (1975), and Gaster & Grant (1975). These disturbances were therefore defined as being 'weak' because the transient and the effects of the generation of vertical vorticity by the three-dimensional initial conditions ultimately decayed owing to viscous forces, and the long-time structure of the disturbance was the Orr–Sommerfeld wave packet. (This behaviour is not restricted to linear disturbances, since weak nonlinearities were observed in Part 1 which did not effect the overall decay of the transient or the growth of the wave packet.)

At higher amplitudes and/or Reynolds numbers, we might expect the disturbance's evolution to be quite different, and it is this regime that we explore in this paper. The linear studies indicate that the disturbance velocities can become quite large (much larger than the initial disturbance) and if the initial amplitude is sufficiently high, or if viscosity is sufficiently weak, the disturbance will achieve an amplitude at which strong nonlinear effects are important, before the transient decays owing to viscous effects. The initial growth of the disturbance may nevertheless be dominated by the linear mechanism of vertical vorticity generation. However, instead of the transient decay and slow wavepacket growth that characterizes the long-time evolution of the weak disturbances, we shall show that

these 'strong' disturbances become dominated by the effects of the nonlinear growth and subsequent breakdown of the transient part of the disturbance.

There are two ways in which one might observe nonlinear effects. The first is the nonlinear growth of the primary disturbance which may end either in some nonlinear equilibrium state or in the breakdown of the laminar flow into a turbulent spot. This kind of nonlinear growth provides a 'platform' for the second nonlinear effect, namely the growth of secondary instabilities. If the primary disturbance becomes strong enough and is sufficiently long-lasting, then it will result in a locally distorted mean profile. This distorted mean profile may be unstable to small scales, allowing high-frequency oscillations to grow, therefore contributing to the local breakdown of the laminar flow. In the results discussed in Part 1 and in those of Henningson (1988), the particular initial conditions considered gave rise to an internal shear layer which was quite persistent as the disturbance travelled downstream. At the higher amplitudes considered in this study, we shall show that, for similar initial conditions, the inclined shear layer that forms does indeed grow nonlinearly, and that the nonlinear distortion of the Blasius profile supports small-scale secondary oscillations.

We have chosen to study the evolution of these 'strong' disturbances through direct numerical simulation. This approach has the advantage of giving the velocity field at every point in the domain, which enables us to examine in detail the structure of the disturbed flow, the two-dimensional spatial power spectra of the velocity components and the form of the observed nonlinear interactions. Experimental measurements of the nonlinear evolution of an isolated disturbance have also been completed (Breuer 1988), but they do not add significantly to the results presented here.

The majority of the results concern the evolution of 'positive' disturbances. The term 'positive' simply means that the form of the initial disturbance is such that it forms an internal shear layer. In §4 the evolution of 'negative' disturbances (i.e. disturbances of equal strength and structure but of opposite sign) is compared with the results for the positive disturbances. Finally, in §5, the effect of initial spanwise scale is discussed and the results from two additional simulations are used to assess the effect of changing the initial spanwise scale on the evolution of the disturbance and how the nonlinear mechanisms scale with the dimension of the initial disturbance.

## 2. Numerical scheme

The initial-value problem was solved numerically using a Navier–Stokes boundary-layer code developed by Spalart (1986). The boundary-layer code is designed to solve the three-dimensional, incompressible time-dependent Navier–Stokes equations for the flow over a flat plate. The boundary conditions in the horizontal plane are periodic, and a Fourier decomposition is used in the $x$- and $z$-planes. (Here $x$ defines the downstream direction, $y$ the direction normal to the wall and $z$ the spanwise direction.) In the wall-normal direction, the semi-infinite half-plane, $y = 0$ to $\infty$, is mapped onto a finite domain and a decomposition using Jacobi polynomials is used in this direction. The flow is required to be zero at the wall and equal to $U_\infty$ in the free stream. This representation of the vertical direction has been shown by Spalart (1986) to be very efficient and accurate with remarkably few modes. The periodic boundary condition in the $x$-direction requires that the mean flow be approximated as being parallel (this also implies that the simulation is a temporal rather than spatial one). However, in order to provide some correction for this, the computational

box is actually moving at a constant speed equal to the average propagation speed of the disturbance and the boundary layer does grow as the disturbance travels downstream. Thus, although the boundary-layer height is constant from the left side of the computational domain to the right side, it does increase as time advances. For the present results, the effect of this correction is minor since the disturbance is only followed for about $50\delta^*$, over which distance there is minimal boundary-layer growth. The code has been used successfully to simulate transition induced by a vibrating ribbon (Spalart & Yang 1987) as well as a turbulent spot (Henningson, Spalart & Kim 1987).

For the results presented here, the calculations were initiated at a Reynolds number based on displacement thickness, $Re_{\delta^*} = 950$ (this will increase as the disturbance travels downstream). This corresponded to the Reynolds number used in the experimental results presented in Part 1. The computations used a $128 \times 35 \times 128$ grid (in the $x$-, $y$- and $z$-directions respectively), and the computational box was $100\delta^* \times 50\delta^*$ in the $x$- and $z$-directions respectively. This resolution was found to be more than sufficient to resolve the relevant scales (Spalart 1988 used a $128 \times 50 \times 96$ grid for a *fully turbulent* flow at $Re_\theta = 500$). Each time-step took about 15 s of CPU time running on a Cray X-MP-48, and about 50 time-steps were needed to advance the solution 100 non-dimensional time units, $tU_\infty/\delta^*$. To conserve computational time, only disturbances symmetric about $z = 0$ were considered. This restriction reduces the computational time required to compute the flow field although it does inhibit certain 'sinuous' instability modes. The possible consequences of this symmetry constraint are discussed in §3.3.

### 2.1. *Initial conditions*

The initial disturbance used consisted of two pairs of counter-rotating eddies defined by the stream function:

$$u = 0; \quad v = -\frac{\partial \Psi}{\partial z}; \quad w = \frac{\partial \Psi}{\partial y}, \tag{1}$$

where

$$\Psi = A\bar{x}\bar{z}\bar{y}^3 \, \mathrm{e}^{-\bar{x}^2-\bar{y}^2-\bar{z}^2} \tag{2}$$

and $\bar{x}, \bar{y}, \bar{z}$ are the normal Cartesian coordinates scaled by $l_x$, $l_y$ and $l_z$:

$$\bar{x} = x/l_x; \quad \bar{y} = y/l_y; \quad \bar{z} = z/l_z. \tag{3}$$

For the present results the scaling lengths used were: $l_x = 5\delta^*$, $l_y = 1.2\delta^*$, and $l_z = 6\delta^*$; chosen so as to be consistent with the results for the weak disturbances described in Part 1. For a more detailed discussion concerning the choice of initial disturbance, the reader is referred to Part 1, although the effect of changes in $l_z$ is discussed in §5.

The disturbance was placed at $x = 0, z = 0$ at time $t = 0$ and the flow field was integrated forward in time. The value for the amplitude factor used in the initial conditions was $A = 0.2$. This value corresponded to an initial peak-to-peak $v$ perturbation of 0.5% of $U_\infty$.

## 3. Results for positive disturbances

### 3.1. *Streamwise velocity*

The series of plots shown in figure 1 show representative frames of the streamwise perturbation velocity field in the $(x, y)$-plane at $z = 0$. The picture in the first frame shows the development of an inclined shear layer structure and is very similar in character to the results seen for the initial behaviour of the low-amplitude disturbance discussed in Part 1. This behaviour can be explained by the linear, three-

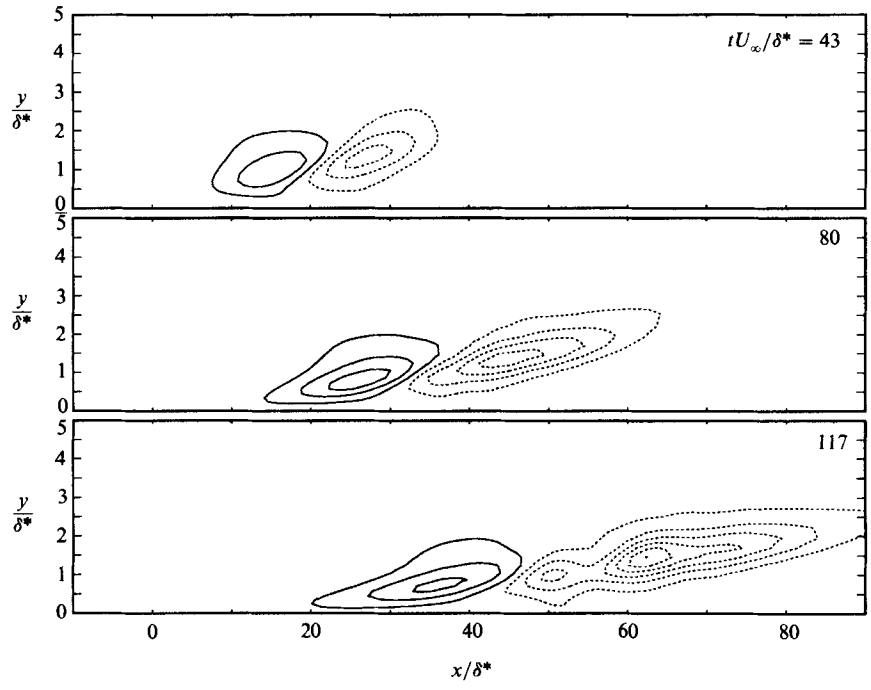


FIGURE 1. Contours of streamwise perturbation velocity in the $(x, y)$-plane at the centreline, $z = 0$. Contour spacing: $0.02U_\infty$. In this and subsequent similar figures solid lines represent positive contours, dotted lines represent negative contours.

dimensional liftup mechanism. The motion of the initial eddies creates two adjoining regions of fluid, a low-speed region, caused by the pushing up of low-speed fluid from close to the wall, and a high-speed region further upstream caused by the pulling down of high-speed fluid. The action of the mean shear tilts the structure over and stretches it, forming an internal shear layer. The shear layer structure is typical of the transient part of the disturbance since it travels at the local mean velocity and is not wave-like in character. Despite the fact that there was initially no streamwise perturbation, the levels of $u$ are quite high, even after a short time: the peak-to-peak perturbation at $tU/\delta^* = 43$ is of the order of 5% of $U_\infty$ and as the disturbance travels downstream, the amplitude of $u$ grows at a slow rate until it begins to rise sharply at $tU/\delta^* = 117$. This is in agreement with Gustavsson (1978) and the linear results of Part 1 which indicate that a small vertical velocity can produce very large-scale horizontal velocities through the three-dimensional transient growth. At later times, there are some new features that were not seen in the low-amplitude results. At $tU/\delta^* = 117$, a 'necking' of the structure has appeared at $x/\delta^* = 55$. This necking was observed to intensify at later times. As we shall see, this is due to a secondary instability which is growing on the 'back' of the shear layer and causing the structure to break down. As the disturbance progresses, it is the downstream side which intensifies while the upstream side, consisting of locally accelerated fluid, remains at an essentially constant amplitude, and even decays at later times. This is also consistent with the results from the linear inviscid calculations in Part 1.

The spanwise structure of the disturbance is shown in figure 2. Initially the disturbance structure reflects the vertical movement of fluid particles by the initial conditions: The low-speed regions are formed by the upward motion of the initial

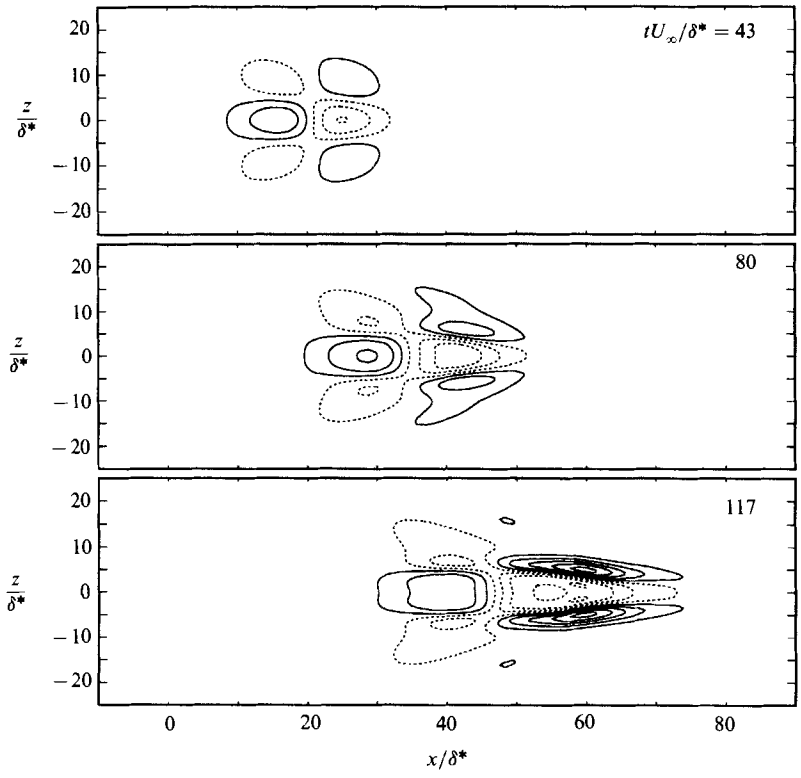


FIGURE 2. Contours of streamwise perturbation velocity in the $(x, z)$-plane at $y/\delta^* = 1.05$. Contour spacing: $0.02U_\infty$.

eddies while the high-speed regions result from the pulling down of high-momentum fluid by the downward motion of the initial eddies. This is also typical of the transient portion of a localized disturbance and several similarities with the low-amplitude results can be seen. As time increases, the wave part of the disturbance becomes visible as a surrounding wave packet develops at the edges of the disturbance and grows slowly, as was seen in the weak disturbance. The most prominent feature that is new to the high-amplitude disturbance is the development of the strong spanwise shear layers and the long, thin regions of high-speed fluid that straddle the central low-speed core of the disturbance as shown in figure 2. As with the necking observed in figure 1, these streaks became more intense at later times. Although the wave packet seen in the linear calculations accompanying the transient structure is also present in the full simulations, by $tU/\delta^* = 99$ it no longer contributes significantly to the structure of the disturbance and is hardly visible since it falls below the level of the lowest contour. From that time, the waves are only a low-amplitude addition to the main part of the disturbance which has evolved from the transient portion of the disturbance. The overall growth of the disturbance was found by computing the evolution of the maximum streamwise perturbation velocity with time. It was found that $u_{\max}$ grow approximately linearly from zero at $tU/\delta^* = 0$ to a level of about 20% of $U_\infty$ at $tU/\delta^* = 100$. At later times, $u_{\max}$ increased sharply, reaching 80% of $U_\infty$ by $tU/\delta^* = 200$.

Based on the vertical and the spanwise structure of the streamwise component of velocity, we can see that the two regions of strong shear have developed in the flow – one in the vertical direction, centred at $z = 0$ and two regions of strong spanwise

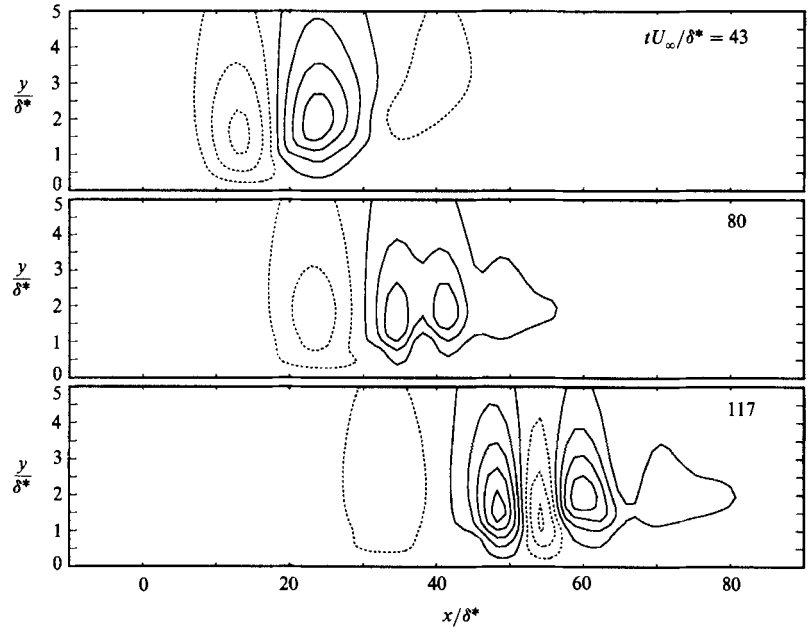


FIGURE 3. Contours of vertical velocity in the $(x, y)$-plane at the centreline, $z = 0$. Contour spacing: $0.002U_\infty$.

shear, $\partial u/\partial z$, on either side of the centreline. The first is directly a linear effect, since it was observed in the linear calculations of Part 1. The second was qualitatively present in the linear model in a very weak form, but the strong spanwise shear layer that we observe is primarily a nonlinear effect that is unique to the stronger disturbance. Although the magnitude of the spanwise shear does become quite large as the long streaks of high- and low-speed fluid intensify, it never exceeds the magnitude of the shear in the $y$-direction. By calculating the shear strength in both the spanwise and vertical directions, we find that the maximum spanwise shear strength normalized by the mean shear, $\partial U/\partial y$, at the wall is still only 0.245 at $tU/\delta^* = 136$. In contrast, the maximum vertical shear strength at the centre of the inclined shear layer is actually greater than the mean shear at the wall.

Both the strength of these perturbations, and their permanence as the disturbance evolves contribute to the formation of locally inflectional mean velocity profiles. The vertical shear at the centreline creates an inflectional profile in $y$, while the spanwise shear creates an inflectional profile in $z$. This raises the possibility of the growth of a secondary instability, although for this flow, in which there are strong shears in both the $y$- and $z$-directions, it is as yet unclear with which shear the secondary instability will be primarily associated. This question will be addressed in the later discussion.

### 3.2. *Vertical velocity*

A contour plot illustrating the centreline structure of the vertical velocity field is shown in figure 3, and the distinction between the horizontal and vertical velocity fields that was seen in Part 1 is made clear once again when we compare the $v$-field with the $u$-field. The normal component here shows none of the structure of the streamwise component and the internal shear layer that the liftup has created. Whereas the $u$-perturbations are confined to the boundary layer ($y/\delta^* < 3$), the normal velocity extends well into the free stream before decaying. This difference

makes sense when one recalls the results from Part 1 in which the vertical vorticity was shown to make the dominant contribution to the horizontal velocities. This contribution is non-zero only in the presence of a mean shear and thus the horizontal disturbance velocities will be confined to the boundary layer where $U' \neq 0$. In contrast to this, the vertical velocity component is governed (in the linear case) by the Orr–Sommerfeld equation whose solutions decay in the free stream as $e^{-ky}$, thus extending well beyond the edge of the boundary layer. Of course, there is a wave component to the horizontal velocities that extends into the free stream and behaves in a similar fashion to the $v$-component, but it is much weaker than the transient portion that is excited in the shear region and is an order of magnitude smaller than the shear-layer perturbations and thus is not seen in the contour plots at the current scaling.

In the linear inviscid problem studied by Gustavsson (1978), the transient part of $v$ was observed to decay like $1/t$ moving with the disturbance. In the viscous problem considered here, we would still expect the transient part of $v$ to decay, although the decay rate will not necessarily be the same. This decay is qualitatively reproduced in figure 3, but only for the upstream side of the disturbance. In that region, the negative $v$-perturbation, corresponding to an accelerated (and therefore stabilized) mean flow, does not develop any wave structure and is simply advected downstream, unchanged (and unstretched), slowly decaying in amplitude as time progresses. However, on the downstream side of the disturbance, the structure does not decay but, rather, grows in amplitude. Here we see more evidence of the growth of a secondary instability associated with the distorted mean profile. The waviness in the contour lines at $tU/\delta^* = 80$ illustrates the initial stages of this wave and as time increases the instability grows and expands until by $tU/\delta^* = 117$ it fills the entire vertical structure of the disturbance. Gustavsson (1978) commented that because the liftup effect is only observed in the streamwise velocity and not in the vertical velocity, it should be much easier to see wave phenomena in the $v$-component because they will not be swamped by the dominant liftup effects. This is illustrated well here since the streamwise contour plots did not show any clear evidence of a secondary instability, and only at $tU/\delta^* = 117$ were we able to see any real changes from the results of the linear theory. In contrast to this, the vertical component, because of its lower amplitude and lack of 'contamination' by the liftup effect, indicates the secondary wave growth at a much earlier time and with more clarity. (In fact, the wave growth was clearly seen in the $v$-component at the even earlier time of $tU/\delta^* = 62$.)

The spanwise structure of the $v$-component at $y/\delta^* = 1.05$ (figure 4) also reflects the secondary wave growing along the centreline. The secondary wave first appears at $t = 62$, indicated by the splitting of the central contour from one island into two. Initially it appears to be almost two-dimensional, but as the wave packet develops, the region of maximum amplitude shifts from the centreline to two peaks on either side of the centreline. Although the mechanism behind this development is not clear, it is qualitatively similar to what was observed in the weak-disturbance experimental measurements in Part 1, in which the maximum positive streamwise perturbation shifted from the centreline to two off-centre peaks. Gaster & Grant (1975) also observed this splitting in the later stages of the growth of a linear wave packet in a boundary layer and commented that it was probably due to nonlinear effects.

In addition to the secondary instability, the contour plots of the $v$-component also reflect the streamwise streaks that were observed in the $u$-component. These streaks develop in two ways. The first is from the intensification of the negative lobes on

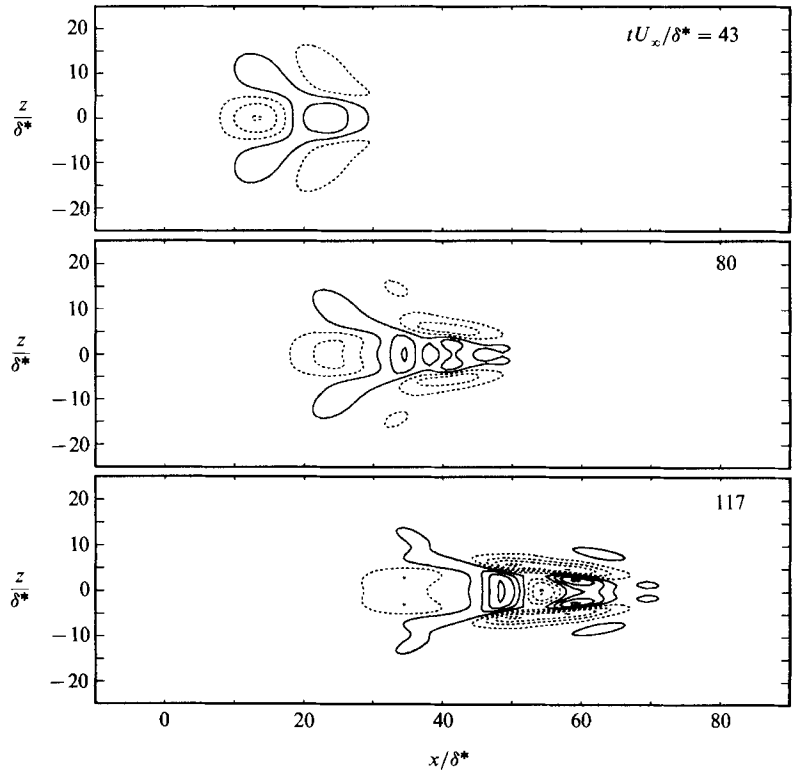


FIGURE 4. Contours of vertical velocity in the $(x, z)$-plane at $y/\delta^* = 1.05$. Contour spacing: $0.002U_\infty$.

either side of the central core. These correspond exactly to the intensification of the positive side lobes in the $u$-velocity and emphasizes the association between the streamwise perturbation and the normal perturbations through the linear liftup effect. Secondly, the streamwise streaks develop further through the growth of the two positive peaks that have formed in the central core from the secondary instability.

In order to determine how these secondary oscillations correlate with the strong shear layers, we must determine the amplitude distribution of the wave packet in the flow field. This is a somewhat subtle problem since we need a method with which to separate the secondary oscillations from both the base flow (the undisturbed Blasius profile) *and* the primary disturbance (the shear layers created by the initial counter-rotating eddies). It turns out that this is not at all difficult. By examining the power spectra of $v$ and of $w$ at fixed values of $y$, it is immediately apparent that the streamwise wavenumbers that characterize the secondary oscillations are higher and quite distinct from the wavenumbers that represent the primary disturbance and the mean flow (this is shown in more detail in the following section which discusses the power spectra of $v$ and by figure 7). Thus, by filtering out all of the energy contained in the lower wavenumbers, we can very effectively isolate the structure of the secondary oscillations.

This was applied to the data field at $tU/\delta^* = 80$, filtering out everything below $\alpha\delta^* = 0.55$, where $\alpha$ is the streamwise wavenumber, and taking the maximum peak-to-peak value of the resultant wavepacket in $x$ as a characteristic value of the

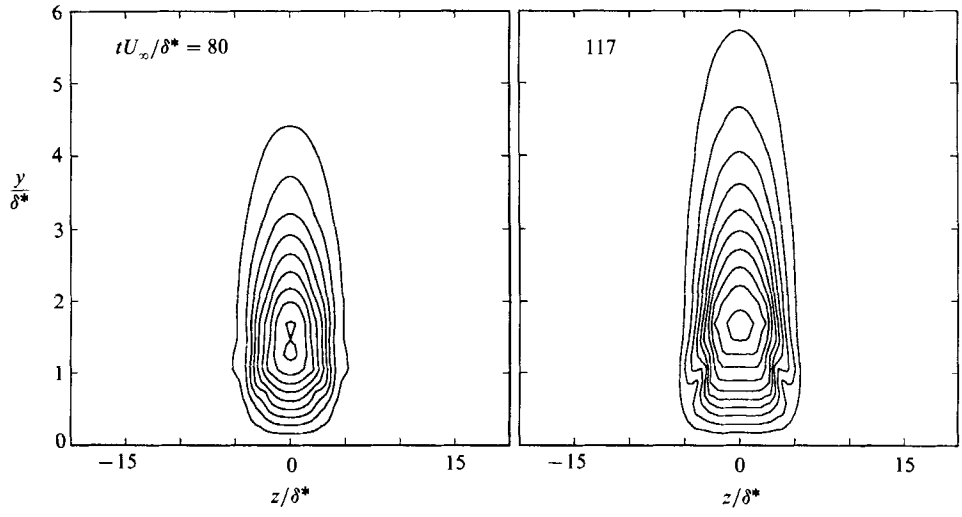


FIGURE 5. Amplitude distribution of secondary oscillations in $v$ in the cross-stream plane at $t = 80$ and $t = 117$, using the maximum value in $x$. Contour spacings are $0.0005U_\infty$ and $0.001U_\infty$ respectively.

oscillation amplitude at each $y, z$ location. This resulted in a measure of the amplitude distribution of the oscillations in $v$ and is shown in figure 5, along with the amplitude distribution of $v$ at $tU/\delta^* = 117$ (filtered at $\alpha\delta^* = 0.4$). Two features are worth noting. First, for both times, the maximum amplitude is located on the centreline and at a height of about $y/\delta^* = 1.5$. By referring to the streamwise disturbance velocity contours at the same times (figure 1*b*, *c*), we see that this location corresponds exactly to the region of maximum vertical shear. The oscillations are completely confined to the central portion of the disturbance, the region where we observe the vertical shear layer structure in $u$, while the region of strong spanwise shear (at $z/\delta^* \approx 3.5$) does not seem to leave any mark on the amplitude of the $v$-oscillations. This leaves little doubt that the oscillations that we observe are associated with the vertical shear, and are not affected by the spanwise shear layer. The second feature to note is the vertical structure of the oscillations. The waves extend well beyond the boundary-layer height and into the free stream, decaying slowly with $y$. This decay was found to be exponential, with a decay rate almost exactly equal to the dominant wavenumber of the disturbance ($\alpha\delta^* = 0.85$ at $tU/\delta^* = 80$, and $\alpha\delta^* = 0.5$ at $tU/\delta^* = 117$). This free-stream structure is consistent with the idea that the oscillations arise from an instability wave developing on the distorted mean profile and suggests that the amplitude distribution of $v$ is closely related to the linear eigenfunction that results from the linear stability analysis based on the distorted mean profile.

This was confirmed by calculating the Orr–Sommerfeld eigenfunction that corresponds to this locally distorted mean flow. The eigenfunction was calculated as follows. The streamwise velocity component at $x/\delta^* = 33, z/\delta^* = 0$ was extracted from the numerically simulated velocity field at $tU/\delta^* = 62$. This profile was filtered, yielding a smooth velocity profile which was representative of the distorted mean field at the centre of the inclined shear layer and at the same location where we observe waves to grow. The Orr–Sommerfeld equation was then solved numerically using this derived mean profile, and taking $\alpha = 1$ for the wavenumber, since this is the wavenumber of the observed instability. This calculation should be regarded

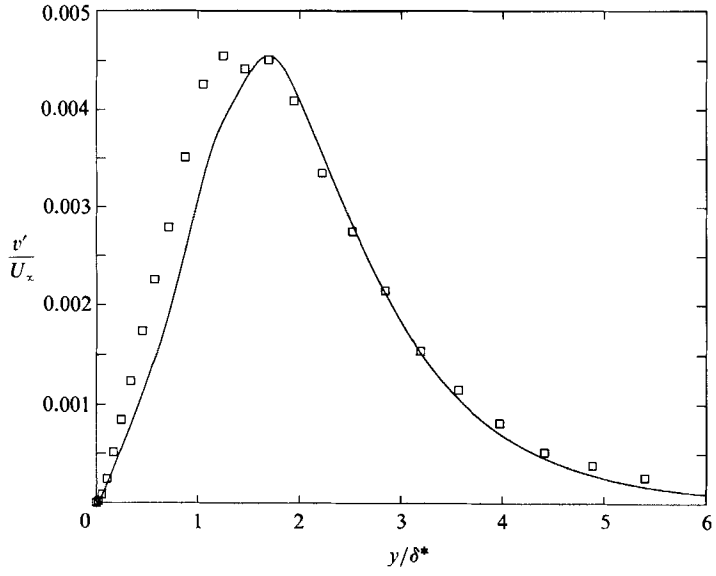


FIGURE 6. The solid line depicts the Orr–Sommerfeld eigenfunction calculated using the mean profile extracted from the simulation data at $x = 33$, $z = 0$, $t = 62$. The symbols show the actual distribution of the secondary oscillations of $v$ extracted from the simulated flow at the same location and time.

with some caution. The derivation of the Orr–Sommerfeld equation is based on a steady, uniform and parallel mean flow, none of which applies to the present case! However, the distorted mean flow, generated by the primary disturbance, evolves quite slowly and is fairly uniform at $x/\delta^* = 33, z/\delta^* = 0$ (relative to the scale of the instability wave considered) and thus a quasi-steady, quasi-uniform approximation seems reasonable, at least as a first approximation. The resultant eigenfunction, along with the observed $v'$ distribution at the same $x, z$ location is plotted in figure 6. The position of the maximum and the exponential decay in the free stream are both well represented by the calculated linear eigenfunction. The numerically extracted data shows a double peak at the maximum, which indicates that the single-mode linear approximation is not completely valid, but nevertheless the agreement is quite good considering the simplicity of the model.

### 3.2.1. *Power spectra of v*

Both of the nonlinear effects that we have observed, namely the development of long streamwise streaks of fluid, and the growth of secondary instabilities on the distorted mean profile, can be clearly seen by examining the power spectra of the velocity field for the disturbance. The two-dimensional spatial power spectra for the $v$-field at $y/\delta^* = 1.05$ are shown in figure 7. The horizontal axis depicts the streamwise wavenumber $\alpha$ (non-dimensionalized by $\delta^*$), while the vertical axis depicts the spanwise wavenumber, $\beta$, similarly non-dimensionalized. The spectrum at $tU/\delta^*$ has the oval shape corresponding to the initial conditions, but by $tU/\delta^* = 80$ we see that a peak has emerged at $\alpha\delta^* = 0.2, \beta\delta^* = 1.3$. This wave angle corresponds to the emergence of the two oblique strips of downward-moving fluid that have appeared on either side of the centreline in figure 4(*b*), and as they intensify at later times, the peak in the power spectrum also intensifies. As the structure grows, it is elongated (by the tilting and stretching of the mean shear) and so the

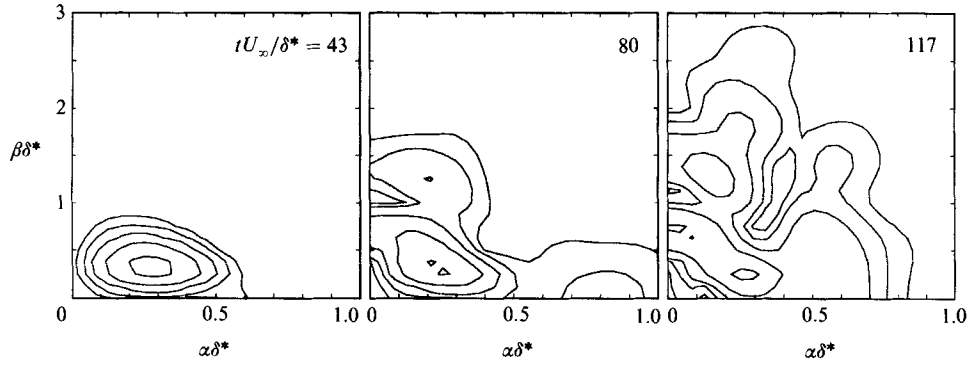


FIGURE 7. Two-dimensional spatial power spectra of the $v$ component of velocity at $y/\delta^* = 1.05$. $\alpha$ represents the streamwise wavenumber, $\beta$ represents the spanwise wavenumber. Contours are plotted on an arbitrary logarithmic scale.

peak moves towards a lower value of $\alpha\delta^*$. By $tU/\delta^* = 117$, a second oblique structure is beginning to emerge, again at $\alpha\delta^* = 0.2$ but at a higher spanwise wavenumber: $\beta\delta^* = 2.5$. On examination of figure 4(*c*), it becomes clear that the original spanwise streak has subdivided into two smaller 'strips', each with a sharper spanwise gradient than the first, hence the higher value for $\beta\delta^*$. The spectra seem to indicate that this process seems to be repeating itself in a cascade: each new peak in the spectrum forming a platform from which the next peak develops at a smaller spanwise scale. By reading from the power spectra at $tU/\delta^* = 136$ (not shown here) we have found that the values of $(\alpha\delta^*, \beta\delta^*)$ at each peak are approximately: $(0, 0.7)$, $(0.1, 1.3)$, $(0.2, 2.0)$ etc., suggesting that each peak is a multiple of the first spanwise peak and that the nonlinearity serves to introduce higher harmonics as time progresses. This progression is just the generation of harmonics that is commonly seen in nonlinear stability theory (for example, Stuart 1960). By the later times, the distinct peaks in the spectrum were observed to be merging together and we would expect that, at some later point, the spectrum will eventually become continuous and the disturbance will have degenerated into a turbulent spot.

The second nonlinear process that was observed in the velocity contours – the secondary wave growth – is also reflected in the power spectra of $v$. Starting at $tU/\delta^* = 80$ a peak appears at $\alpha\delta^* = 0.85, \beta\delta^* = 0$. This corresponds to the two-dimensional wave packet that was observed growing on the back of the distorted mean profile at $z/\delta^* = 0$. We should note here that the primary disturbance and the secondary instability clearly occupy quite distinct wavenumber regimes and that the filtering process that was used in the previous section in order to obtain the instability amplitude distribution is therefore valid.

As the disturbance progresses, the wavenumber about which the secondary instability is centred decreases, along with the rest of the disturbance spectrum, indicating that the wave stretches along with the structure. In addition to this, the peak of the wave packet moves off the $\beta\delta^* = 0$ axis, corresponding to the previous observation in the velocity field that the maxima of the wave packet moved off the centreline. This behaviour is also consistent with the spectra obtained by Gaster & Grant (1975). At $tU/\delta^* = 117$ a subsequent peak at $\alpha\delta^* = 0.6$ and $\beta\delta^* = 1.5$ has appeared, and at $tU/\delta^* = 136$, a third peak at $\alpha\delta^* = 0.5, \beta\delta^* = 2$ was also observed to be emerging, indicating that the wave packet itself had begun to participate in nonlinear interactions. This evolution of the secondary instability, and the

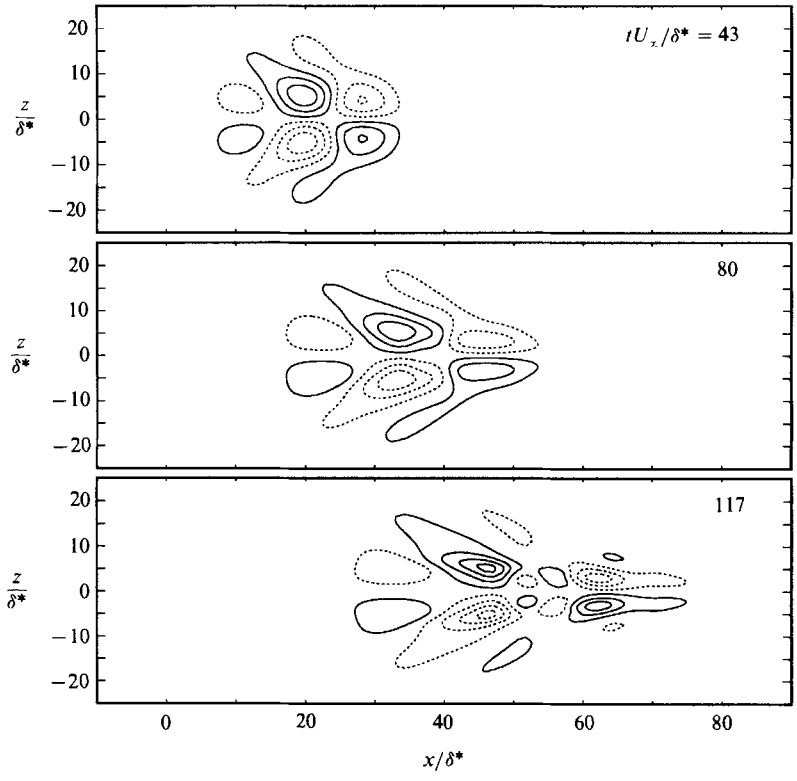


FIGURE 8. Contours of spanwise velocity perturbations in the $(x, z)$-plane at $y/\delta^* = 1.05$. Contour spacing: $0.01U_\infty$.

appearance of new peaks at successively higher spanwise wavenumbers is identical to what we have already observed in conjunction with the nonlinear development of the primary disturbance and suggests that the same nonlinear mechanism that generated the oblique strips from the primary disturbance might also be responsible for the nonlinear evolution of the secondary instability.

### 3.3. *Spanwise velocity*

Contour plots of the spanwise velocity component are shown in figure 8 which depicts the structure of $w$ in the $(x, z)$-plane at a height of $y/\delta^* = 1.05$. At $tU/\delta^* = 43$ we see four main lobes, which is essentially the structure of the initial perturbations. In addition we see the signs of a swept-back wave packet which is growing on the sides. As the disturbance propagates downstream, the structure remains essentially the same except that it elongates as it advances. One should remember that, in common with the streamwise velocity, linear theory predicts that the spanwise velocity is also dominated by the liftup effect, and thus the core of the $w$-structure is advected at the local mean velocity. As we have seen, this results in the stretching of the disturbance by the action of the background shear profile and this is what is observed here. The waves on the sides of the structure are the linearly amplified dispersive portion of the disturbance and, as such, travel at typical wave speeds that are somewhat slower than the local mean velocity at this height in the boundary layer. This difference in propagation speeds is confirmed in figure 8 as we see that the edges of the disturbance are lagging the core as the whole structure advances.

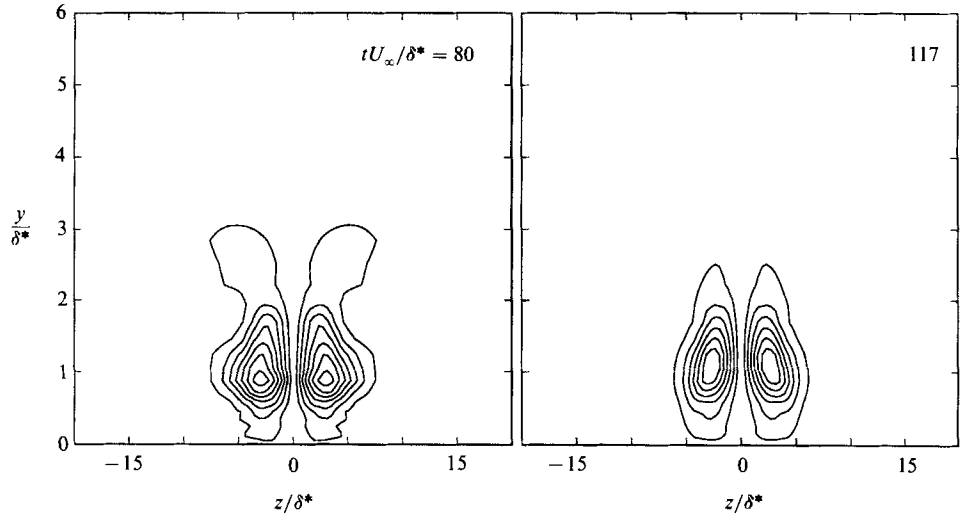


FIGURE 9. Amplitude distribution of secondary oscillations in $w$ in the cross-stream plane at $t = 80$ and $t = 117$ using the maximum value in $x$. Contour spacings are $0.001U_\infty$ and $0.005U_\infty$ respectively.

By $tU/\delta^* = 99$, and at subsequent times, an additional feature has become apparent in the $w$-contours. This is the development of additional contour lines in the centre of the disturbance and on either side of the line of symmetry. These islands represent a wave that is growing in the $w$-component. We had already anticipated that the strong shear layers that were observed in the $u$-velocity would render the flow susceptible to secondary instabilities. These have already been observed in the $v$-component, which in that case were associated with the inflectional vertical profile along the centreline. Those oscillations in $v$ showed no correlation with the spanwise shear in the $u$-velocity. However, from these contour plots, it appears that the oscillations in $w$ are centred in the regions away from the centreline and close to the regions of high spanwise shear $\partial u/\partial z$. It is therefore possible that these oscillations are correlated with the spanwise structure of the distorted mean flow.

In order to determine more precisely the spatial structure of the oscillations in $w$, the amplitude distribution of the secondary oscillations in $w$ was computed using the same technique employed for the secondary instability in $v$. At each $(y, z)$-location, the $w$-signal was filtered using a high-pass filter set at the optimal streamwise wavenumber for each time in order to remove the primary spanwise perturbation while leaving the secondary oscillations untouched. For $tU/\delta^* = 80$, this wavenumber was $\alpha\delta^* = 0.54$, and at $tU/\delta^* = 117, \alpha\delta^* = 0.4$. As before, the maximum perturbation of the filtered signal was taken as the amplitude of the oscillations for that $y, z$ location. The results of this operation are shown in figure 9 in which the amplitude distribution of the secondary spanwise oscillations are plotted for both $tU/\delta^* = 80$ and $tU/\delta^* = 117$. What is apparent is that the maximum in the distribution occurs on either side of the centreline at about $y/\delta^* = 1, z/\delta = 3.5$ which corresponds to the maximum in the spanwise shear $\partial u/\partial z$. At first glance this would seem to indicate that the secondary oscillations in $w$ are indeed correlated with the spanwise shear and not the vertical shear as was the case with the $v$-component. This indication would be in agreement with the results of Swearingen & Blackwelder (1987) who studied the secondary oscillations observed in Görtler vortices. Their

measurements (of the streamwise velocity component) indicated that the instability that grew on the Görtler vortices seemed to be associated more with the spanwise shear $\partial u/\partial z$ than with the normal shear $\partial u/\partial y$. Although the Görtler flow and the present case have important differences (the foremost being that the Görtler flow does not have a strong $x$-dependence), both are characterized by two distinct mean shears (normal and spanwise) and the oscillations that develop as a result of the distorted flow might be correlated with either one of these shear layers.

However, we should proceed with caution, for there are several reasons to believe that, despite the distribution indicated in figure 9, the spanwise shear does not play a major role in the secondary instability process. The calculation presented here has enforced symmetry about the $x$-axis, and this requires that the $w$-field is always antisymmetric about that axis and must be zero at $z/\delta^* = 0$. Thus, any feature observed in the $w$-velocity will have its maximum away from the centreline. It is possible that, if the calculation were repeated without any spanwise symmetry constraint, an instability mode in $w$ may arise at $z/\delta^* = 0$ and alter the observed distribution. (This is planned for future calculations and experiments.) This constraint explains why figure 9 has the observed structure. However, it does not necessarily exclude any importance of the spanwise shear layer.

One aspect of the $w$-waves that indicates that they are associated with the vertical shear is their wavelength. As we noted earlier, the spanwise shear layer strength is considerably smaller than the vertical shear layer strength. Thus, if the $w$-oscillations are associated with the spanwise shear we would expect that the characteristic scale of the $w$ waves would be much longer than the scale of the $v$-oscillations which are associated with the vertical shear. This is not, however, the case and the wavelength of the $w$-oscillations is almost identical to that of the $v$-oscillations, indicating that they are both caused by the vertical shear layer.

Another aspect of this argument concerns the structure of the oscillations far from the disturbance. In the case of the vertical component, the secondary oscillations were observed to decay exponentially in the free stream – a result consistent with ideas from stability theory. In the case of the $w$-oscillations, if they do indeed arise from a spanwise instability, we should see a corresponding behaviour, that is, that $w$ decay exponentially, $w \propto \mathrm{e}^{-kz}$, with $k$ given by the dominant wavenumber of the spanwise oscillation (which we have already noted, is comparable with the dominant wavenumber of the oscillations in $v$). Upon examination of the amplitudes of the $w$-oscillations it is apparent that this is not the case and, as figure 9 indicates, the $w$-oscillations decay much faster, and are confined in both the spanwise and the vertical directions. This would indicate that the observed waves in $w$ are not due to an instability associated with the spanwise shear, but rather are another manifestation of the instability due to the vertical shear layer, perhaps augmented by a cross-flow instability and forced to have the observed bi-modal structure by the symmetry constraints of the numerical procedure. The possibility of a cross-flow instability contributing to the $w$-oscillations is supported by the strong spanwise velocity that is observed on either side of the centreline. At these locations the effective mean profile for linear stability (which is given by $U_e = \alpha U + \beta W$) will be strongly unstable owing to the spanwise velocity component (which is supplied by the primary disturbance field) and we should expect that there will be significant secondary oscillations in that region due to this mechanism.

Of course, as the disturbance grows in both amplitude and structural complexity, the straightforward association between the oscillations and the shear layers becomes more difficult. We should point out that at the later times the interactions

between the vertical and spanwise shear layers in the primary disturbance and the oscillations in $v$ and $w$ (which quickly attain quite large amplitudes) are undoubtably complex. This is emphasized by the appearance of kinks in the contour lines in the distribution of $v$-oscillations at $tU/\delta^* = 117$ (figure 5) which indicate that the application of these simple arguments must be limited.

We do not show the spectra of the $w$-component, but since we know from the velocity contours of $w$ that the spanwise component does not change as dramatically as the $u$- and the $v$-components, we do not expect that the spectra of $w$ will show any new features. The secondary instability that we have just discussed was seen to appear in a very similar manner to that observed in the $v$-component. The waves first appear as a two-dimensional wave packet, centred about $\beta\delta^* = 0$. However, by $tU/\delta^* = 99$ the primary peak is centred at $\alpha\delta^* = 0.65, \beta\delta^* = 0$ but a second peak appears at $\alpha\delta^* = 0.65, \beta\delta^* = 1$. It is interesting to note that whereas the wavepacket in the $v$-component moved off the $\beta\delta^* = 0$ axis, the wave packet in $w$ always remains on the axis. Since the $w$ velocity contours did not show any signs of the streamwise streaky structure that we have seen in the $u$ and $v$, the spectra do not show much else of interest. Apart from the appearance and growth of the secondary oscillations, and the appearance of harmonics at higher values of $\beta$ (in essentially the same way as was observed in the $v$-spectra) the $w$-spectra only show a gradual growth of the disturbance and an increasing complexity.

### 3.4. *The structure of the pressure field*

One of the convenient features of data resulting from numerical simulations is the availability of the pressure field in addition to the velocity field. This is, of course, impossible to achieve in the laboratory where the only pressure data available are at the wall, and even then usually only at a limited number of locations. We might expect that the pressure will depend little on $y$, in accordance with the result from steady-state boundary-layer theory. This is confirmed in figure 10, in which the pressure at the centreline remains approximately constant through the boundary layer, only decaying in the free stream as $y \to \infty$. (Note that the vertical coordinate in figure 10 is stretched, and so the normal gradients are in fact somewhat higher than they appear. Nevertheless, the pressure only begins to change when $y/\delta^* > 2$.) The decay of the pressure in the free stream is predicted by linear inviscid theory in which the pressure in the free stream is linearly related to $\partial v/\partial y$. Since $v$ decays as $e^{-ky}$ in the free stream, the pressure must decay accordingly. The reason for the jaggedness in the pressure contours is not clear, but it is thought that it lies in the numerical error accrued while calculating the pressure from the velocity field. The pressure does not actually appear directly in the equations that are numerically integrated, but is calculated afterwards by solving a Poisson equation. This may have some inaccuracies associated with it which cause the saw-tooth lines in the pressure contours.

It is quite straightforward to show from the inviscid linear theory for the evolution of a three-dimensional disturbance that the Fourier component of pressure, $\tilde{p}$, depends solely on the Fourier component of vertical velocity, $\tilde{v}$, and the mean profile:

$$\tilde{p} = \frac{1}{k^2}\left[\mathrm{i}\alpha U'\tilde{v} - \left(\frac{\partial}{\partial t} + \mathrm{i}\alpha U\right)\tilde{v}_y\right], \tag{4}$$

where $k^2 = \alpha^2 + \beta^2$ and $\alpha$ and $\beta$ are the streamwise and spanwise wavenumbers respectively (for more details on the derivation of this equation, see Part 1). Clearly,

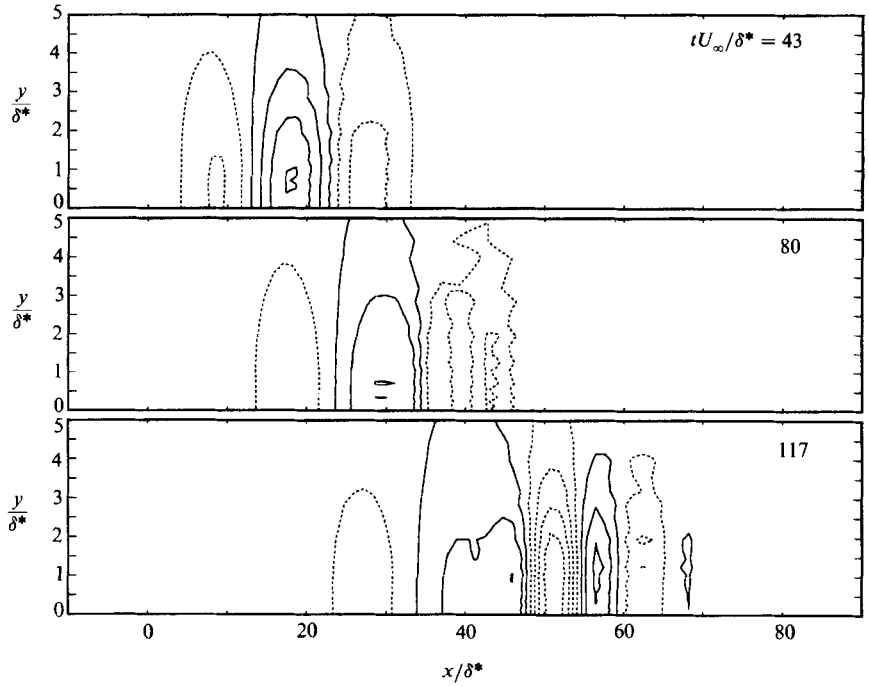


FIGURE 10. Contours of pressure in the $(x, y)$-plane at $z = 0$. Contour spacing: $0.001U_\infty^2/\rho$.

the present results do not derive from a linear flow, and in general the nonlinear effects will include interactions with other velocity components. However, if one compares the pressure contours in figure 10 with the similar plot for the vertical velocity (figure 3), one sees that the two signals are strongly related, and that the pressure peaks coincide with the maxima in the streamwise gradient of the $v$-component. This is exactly the leading term in (4) and suggests that the dominant term in the pressure equation is the mean shear interaction, $U'\partial v/\partial x$. This is in agreement with the results of Johansson, Her & Haritonidis (1987) who investigated the relationship between wall pressure and the velocity field in a fully turbulent boundary layer. They also found that the conditionally averaged wall pressure is closely related to the gradient of the conditionally averaged vertical velocity measured in the buffer region at the same $x$-location.

The spanwise structure of the pressure (figure 11) also reflects the dependence on the streamwise gradient of $v$, although the structure is somewhat more complicated. For the early times, when the gradients in the flow are not very sharp, the pressure peaks do align themselves with the streamwise gradients in $v$. However, at later times, as the flow becomes more complex, this correspondence is not so clear. There does not appear to be any effect on the pressure from the sharp spanwise gradients that are seen in the streamwise disturbance velocity field and we do not observe the strong oblique strips that both the $u$ and the $v$ exhibit (recall that this was also true for the $w$-component of velocity). Referring back to the equation for $\tilde{p}$ given by linear theory (4), this result is also not unexpected, since the pressure depends only weakly on the spanwise gradients in $v$.

Another remark may be made here concerning the oscillations in the $w$-component of velocity. We have seen that the secondary $v$-flow causes a secondary pressure

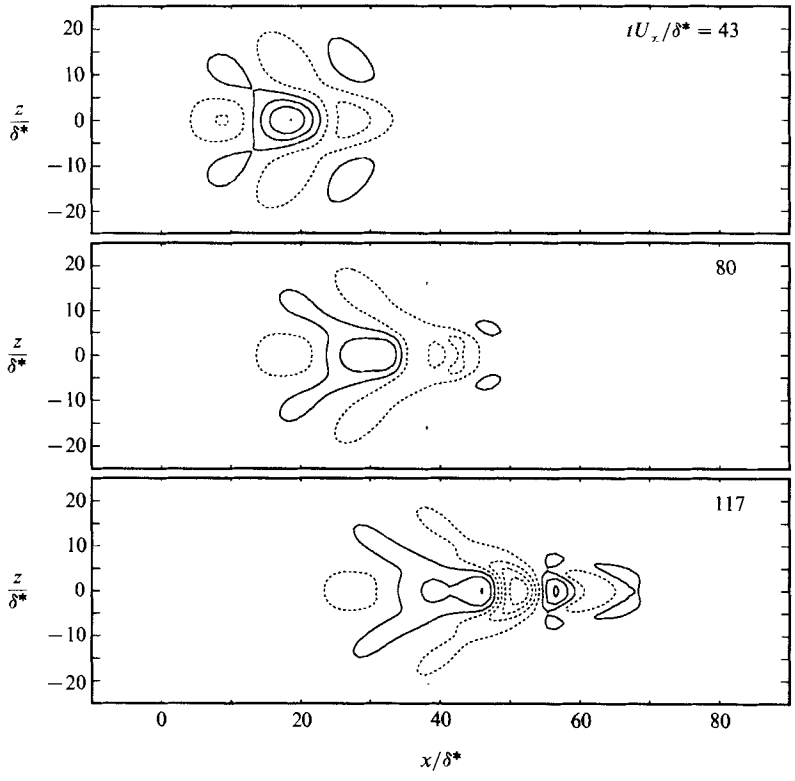


FIGURE 11. Contours of pressure in the $(x, z)$-plane at $y/\delta^* = 1.05$. Contour spacing: $0.001U_\infty^2/\rho$.

distribution, and that the two correlate quite well with each other. The largest spanwise pressure gradients are also seen to correlate with the spanwise edges of the vertical shear layer and it is likely that these spanwise pressure gradients contribute to the $w$ oscillations that were observed in this region of the flow.

## 4. Results for negative disturbances

We shall briefly discuss some results derived from the computation of the initial-value problem for a 'negative' disturbance. This initial disturbance has exactly the same structure and amplitude as the disturbance discussed thus far, but with opposite sign (i.e. taking the amplitude in the stream function to be $A = -0.2$). This kind of comparison was briefly discussed in Part 1 in the context of weak disturbances and it was found that although the positive and negative disturbances had some differences due to a weak nonlinearity, the resultant wave packets (after the transient part had decayed) were identical but of opposite sign. In the present case, the nonlinearity is clearly not weak and we have seen that the disturbance grows dramatically owing to the nonlinear effects of the transient. Thus, we would expect that at this amplitude, the evolution of the two disturbances will differ in a more significant manner. Owing to limited computer resources, the results presented here only cover the time range from $tU/\delta^* = 0$ to 100, and so the results at later times cannot be compared. However, from what results are available, we can still make some worthwhile comparisons.

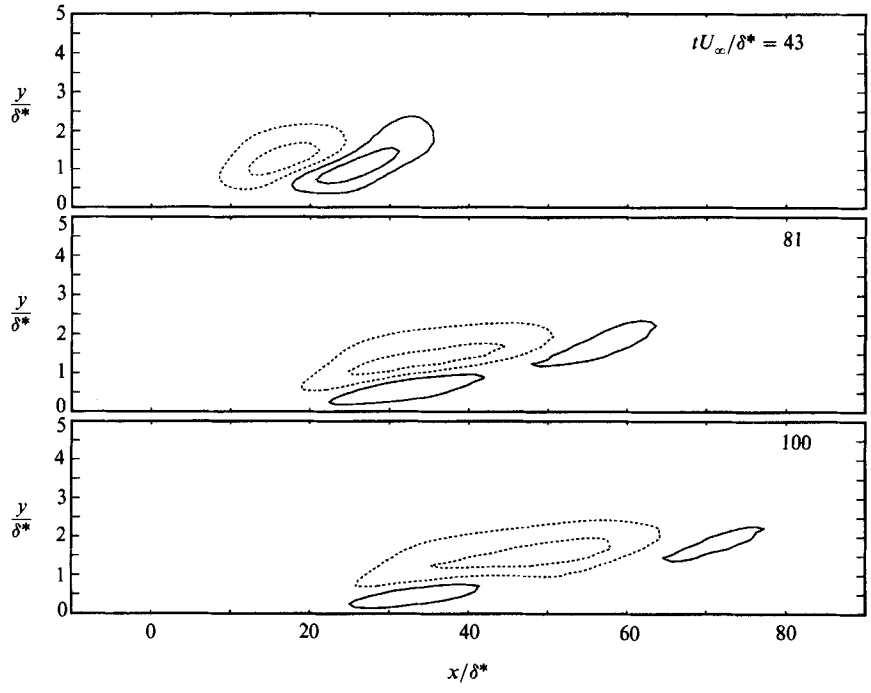


FIGURE 12. Contours of streamwise perturbation velocity in the $(x, y)$-plane at $z = 0$. *Negative* disturbance. Contour spacing: $0.02U_\infty$.

The initial vertical structure of the streamwise perturbation velocity (figure 12) appears to be identical but opposite to the structure of the positive disturbance, and given that the initial liftup mechanism has been shown to be a linear one, this is not surprising. In an identical manner to the positive case, the linear mechanism of the liftup effect, in which the fluid particles move at the local mean velocity, causes the disturbance to elongate and tilt over as the disturbance evolves. The main difference between the two disturbances is that the disturbance structure created here is not an internal shear layer, but rather a locally 'fattened' profile near the wall and a decelerated region in the upper part of the boundary layer. We know that, unlike the previous case, this is not inviscidly unstable, and already we can anticipate that the secondary instability that was observed in the positive disturbance will not be seen in this case (at least not in the same form).

From these cuts through the boundary layer at $z/\delta^* = 0$, it appears that the disturbance does not grow at all. However, figure 13 indicates that the structure does intensify as it evolves, but this time the main growth occurs on either side of the centreline. Qualitatively, the spanwise structure of the negative disturbance does appear somewhat similar to its positive counterpart. We still observe the weak wave field resulting from the initial conditions at the edges of the disturbance and, more importantly, we see the development of the strong streamwise streaks of high- and low-speed fluid and the development of strong spanwise shear layers in the streamwise velocity field. The physical appearance of the disturbance looks very similar to the experimental results of Landahl, Breuer & Haritonidis (1987) who studied this type of disturbance in connection with the control of boundary-layer transition. The similarity in both structure and amplitude serves as a confirmation that the numerical results are accurate.

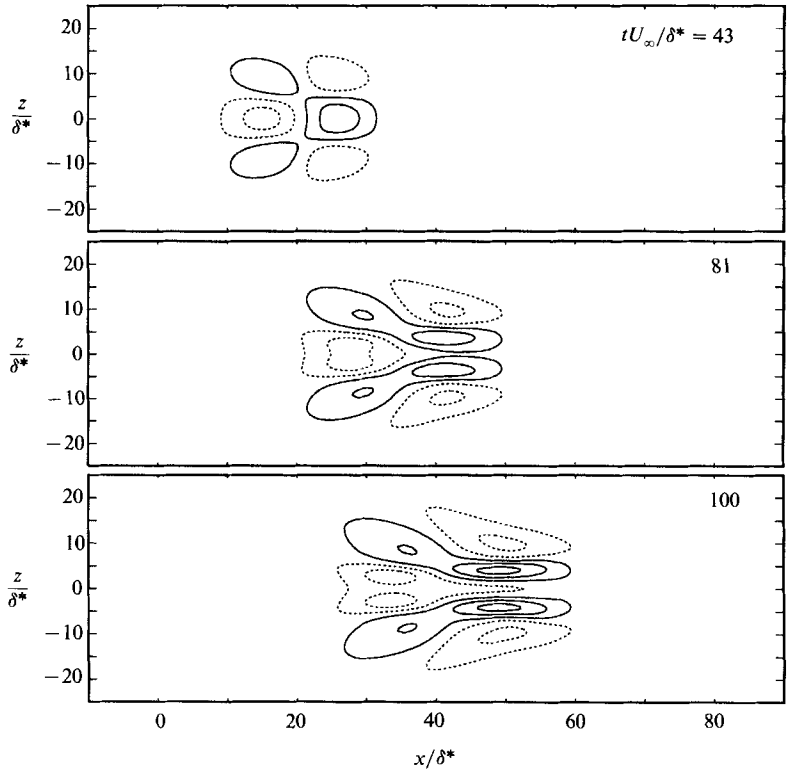


FIGURE 13. Contours of streamwise perturbation velocity in the $(x, z)$-plane at $y/\delta^* = 1.05$. *Negative* disturbance. Contour spacing: $0.02U_\infty$.

The appearance of the streaky structure and the spanwise shear layers suggests that the same nonlinear mechanism that was observed in the positive disturbance is in evidence here. This was confirmed by looking at the spectra of $v$ at $y/\delta^* = 1.05$ for the negative disturbance, which indicated the emergence of a new peak at $\alpha\delta^* = 0.15$, $\beta\delta^* = 1.0$ which is at a similar location in wavenumber space to the peak that emerged in the positive disturbance. (The spectra for the negative disturbance are not shown here because they are so similar in character to the spectra for the positive disturbance presented in figure 7. The only significant differences between the spectra from the positive and negative disturbances are those discussed in the following paragraph.)

Although the central core of the disturbance does not form an inclined shear layer and therefore is not susceptible to a secondary instability, examination of the spectra of $v$ from the negative disturbance did show some signs of secondary oscillations growing in the same manner as was observed for the positive disturbance. The peak representing the secondary oscillations was much weaker than the corresponding peak in the spectra from the positive disturbance, but indisputably present. Upon close examination of the vertical velocity field, the resolution of this paradox becomes clear. While the central part of the negative disturbance does not form an inclined shear layer, the side lobes on either side of the centreline *do* have the same form as the positive disturbance, and they form two inclined shear layers, one on either side of the central region. The amplitude of the side lobes is considerably smaller than the central core, and so the shear layer strength is smaller than what

we observed in the positive disturbance case, but nonetheless, two shear layers are formed and all of the subsequent evolution of the negative disturbance is in relation to these twin disturbances. The secondary oscillations in $v$ are observed at the centres of each disturbance, the high- and low-speed streaks that lead to the strong spanwise shear layers are seen on one side of each shear layer, leading to the observed spanwise structure of the $u$-component. Even the slower overall growth of the negative disturbance (the negative disturbance maintains a maximum streamwise perturbation velocity of only one half that of the positive disturbance from $tU/\delta^* = 0$ to 100) can be explained by the fact that the dynamically significant inclined shear layers are initially weaker in the case of the negative disturbance, since they derived from the side lobes of the initial perturbation.

## 5. The effect of changes in the initial spanwise scale

We have seen thus far in the development of the localized disturbance that the driving forces in the initial growth of the structure result from the transient liftup effect. As the linear theory indicates (see Part 1) this portion of the initial disturbance is inherently associated with the three-dimensional nature, and hence the spanwise scale of the initial disturbance. As the spanwise scale becomes greater, i.e. the initial disturbance becomes more two-dimensional, the liftup effect lessens and the transient modes contain only decaying terms (Gustavsson 1978). Conversely, we would expect that as the three-dimensional nature of the initial field increases, these effects will become more prominent.

In order to investigate the effect of the initial spanwise scale, the flow simulation was repeated at the same Reynolds number and with the same counter-rotating eddies as the perturbation velocity field, but with different initial spanwise dimensions. This is easily accomplished by changing the parameter $l_z$ in the disturbance stream function. For the comparison, the simulation was repeated using $l_z = 3\delta^*$ compared with a value of $6\delta^*$ used in the previously discussed results (the 'base run'). Physically, this had the effect of halving the spanwise scale of the initial eddy structure. If the perturbations are plotted with a $z$-scale expanded by 2, the structure of the initial disturbance is identical. We must, however, be aware of what else changes when the initial spanwise scale is altered. Recalling that the initial vertical velocity is defined as

$$v = \frac{\partial \Psi}{\partial z} = \frac{1}{l_z}\frac{\partial \Psi}{\partial \bar{z}} \tag{5}$$

we see that the magnitude of the initial vertical velocity field must increase as $l_z$ decreases (in order to maintain a constant total mass flow, which is set by the stream-function amplitude $A$). The total energy of the initial disturbance may be found by integrating over all space $v^2 + w^2$ ($u$ is initially zero) and it may be shown that for the chosen stream function, this results in an expression:

$$E \propto A^2 l_x \left(45\epsilon + \frac{33}{\epsilon}\right), \tag{6}$$

where $\epsilon = l_y/l_z$. The first term inside the parentheses comes from the effect of the initial scales on $v$, while the second term represents the effect on $w$. Clearly, many quantities besides energy may be looked at to see how they change as the geometric parameters of the initial conditions vary. For example, the total momentum of the initial perturbations, the maximum spanwise velocity, etc.

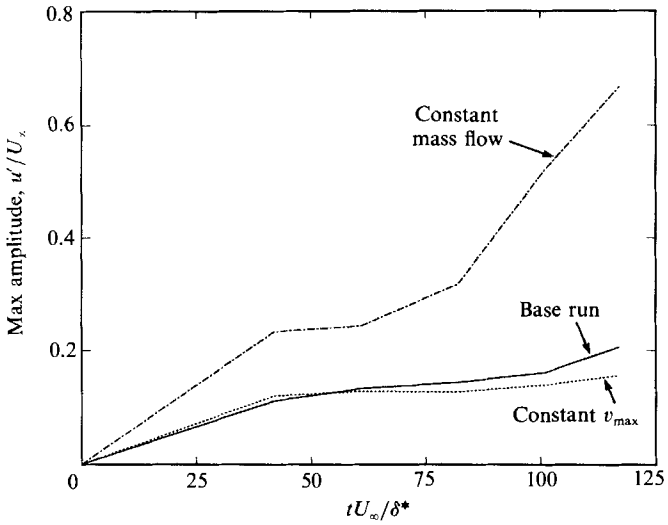


FIGURE 14. Amplitudes of three disturbances with different initial geometries. Solid line: base run; dotted line: constant-$v_{max}$ case; dot-dash line: constant-mass-flow case.

In the present case, two additional simulations were performed to evaluate the effect of spanwise scale. Both of these used the same value of $l_x$ and $l_y$ since it was desirable to change only one geometric scale. In the first comparison, $l_z$ was decreased from 6 to 3 while the amplitude was kept constant at $A = 0.2$. This meant that the mass of fluid moved remained constant, but the initial vertical velocity increased by 100%. The total energy of the initial field actually decreased by 42% (owing to the decreased energy in the $w$-velocities). This run is referred to as the 'constant-mass-flow' run. In the second comparison, both $l_z$ and $A$ were decreased by 50%. This reduced the mass flow by 50% and the total perturbation energy by 86%. However, the amplitude of the initial vertical velocity, which is the primary force for the liftup effect, remained constant. We shall refer to this run as the 'constant-$v_{max}$' run.

In both of the comparison cases examined, the basic structure of the disturbance was the same as we have already seen in the base run discussed previously. The formation of the shear layer, the secondary waves and the nonlinear formation of the streamwise streaks were all observed in the comparison cases and, when plotted with an expanded $z$-scale, their qualitative appearance is identical to the base run which we have already discussed. For this reason, we have not presented contour plots of the velocity field for the comparison runs, but rather we shall concentrate on how the disturbances differ, specifically comparing the overall growth rate of the disturbances and the scaling of the nonlinear effects and secondary instabilities.

### 5.1. *Overall growth of the disturbance*

A comparison of the overall growth rates of the disturbances is shown in figure 14 which shows the maximum $u/U_\infty$ perturbation as a function of time. The base run is shown by the solid line while the comparison runs with reduced initial spanwise scale are shown by the two dotted lines. The first (dot–dashed) shows the constant-mass-flow run, in which the initial vertical velocity was increased by 100% over the base run grows at an extremely rapid rate until $tU/\delta^* = 80$, when its perturbations are about twice as large as those of the base run. After $tU/\delta^* = 80$, it grows at an even faster rate and the velocity contour plots indicate an extremely complex and

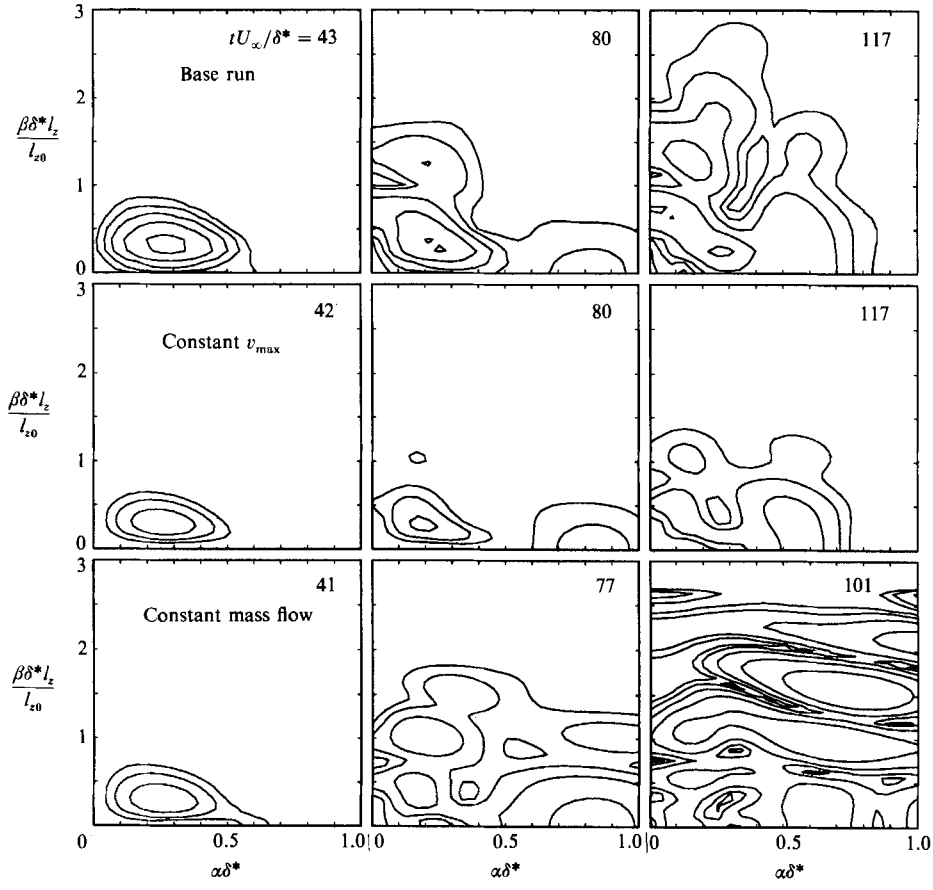


FIGURE 15. Comparison of power spectra of $v$ for calculations with different initial geometries. The contour levels are logarithmic and scaled by the maximum initial vertical velocity.

intricate structure. Although the disturbance's energy was almost half the energy of the base run, the large initial vertical velocity, and the reduced spanwise scale combine to create a disturbance which grows very rapidly. By comparison, the constant-$v$ calculation (shown by a dotted line) grows at approximately the same rate as the base run, *despite the fact that its initial energy is* 85 % *lower*. The fact that the constant-mass-flow growth rate is initially twice the growth rate of the base run, while the constant-$v$ case grows at the same rate suggests that the initial growth rate of the disturbance depends linearly on the amplitude of the vertical velocity of the initial perturbation. This is in agreement with the observed dominance of the liftup mechanism in the disturbance's initial growth which is driven by the vertical movement of fluid particles. Changes in the spanwise dimension and the initial energy of the disturbance are only relevant in so much as they change the initial vertical displacement, which appears to be the dominant factor in the disturbance's initial growth rate.

### 5.2. *The scaling of the nonlinear effects and secondary instabilities*

Figure 15 shows the two-dimensional power spectra of the vertical component of velocity for the base run and both the comparison runs. The vertical scale is the normalized spanwise wavenumber: $\beta\delta^* l_{z0}/l_z$, where $l_{z0}$ is the spanwise dimension of

the disturbance used in the base run. This normalization allows us to see more clearly the scaling of the disturbance with the initial spanwise dimension. The horizontal scale is the normal streamwise wavenumber. The contour levels (which are arbitrary logarithmic levels) are also normalized so that at $tU/\delta^* = 0$ the three initial spectra are identical. At $tU/\delta^* = 42$, the three still appear to be more or less the same. However, the constant-mass-flow case already shows the signs of the secondary instability appearing as a two-dimensional wave at $\alpha\delta^* = 0.6$. By $tU/\delta^* = 80$, both nonlinear effects that were observed in the base run are seen in all three flows. Several comments should be made here. The secondary instability, which is centred along the $\beta\delta^* = 0$ axis, appears at the same value of $\alpha\delta^*$ for all three geometries. This indicates that the spanwise scale does not affect the wavelength of this instability. This is not really surprising since the secondary instability is associated with the shear layer in the normal direction, which would not be affected by the initial spanwise scale. We would expect that this would be dependent on the streamwise scale of the initial disturbance, but this has not yet been investigated. However, the second peak that develops as a result of nonlinear interactions, at $\alpha\delta^* = 0.2, \beta\delta^* l_z = 7$, is at approximately the same location for all three initial configurations, suggesting that this nonlinear interaction is inherently tied to the initial spanwise scale of the disturbance. This also makes sense when one recalls from §3.2.1 that this peak may be identified with the streamwise streaks of high- and low-speed fluid that evolve in the flow and that the spacing of these streak scales with $l_z$.

Although they are not shown here, the two-dimensional power spectra show similar results for the $w$-component of velocity, with some minor differences. The $w$-waves appear at the same values of $\alpha\delta^*$ in all three simulations, indicating that their scale is not affected by the spanwise dimension of the initial disturbance. This is significant because the changes in the initial spanwise scale affect the strength of the spanwise shear layer. That the scale of the $w$-oscillations is not altered by the changes in $l_z$ reinforces the view that the oscillations observed in $w$ are due to the instability of the vertical shear layer and not of the spanwise shear layer. As was observed with the $v$-component, the peaks in the power spectra associated with the direct nonlinear interactions (i.e. the harmonics appearing at higher values of $\beta\delta^*$) *do* scale linearly with $l_z$.

## 6. Conclusions

The evolution of a moderate-amplitude localized disturbance shows many of the qualitative features that have been observed in linear and low-amplitude disturbances. The liftup effect, which is solely a feature of the three-dimensional nature of the initial perturbations, quickly dominates the horizontal perturbation velocities, creating a shear-layer structure which stretches and intensifies as the disturbance progresses. It must be emphasized that this initial behaviour is a purely linear phenomenon despite the moderately high amplitude of the initial disturbance. This is supported by observing how well the initial growth rate of the disturbance scales with the strength of the liftup term when the geometry of the initial disturbance is changed. The dominance of the transient portion of the disturbance due to the liftup effect emphasizes the importance of the three-dimensional nature of the disturbance. The linear equations indicate that even a modest spanwise structure can, in the presence of a strong mean shear, produce large-amplitude horizontal perturbations leading to secondary instabilities and nonlinear intensification of the disturbance.

Despite the initial linear character of the disturbance, nonlinear effects are quick to establish themselves and we see both the distortion of the 'mean' profile and the growth of secondary instabilities as the disturbance evolves. The nonlinear distortion takes the form of strong streaks of high- and low-speed fluid that intensify as the disturbance evolves. In the power spectra of the velocity, these nonlinear effects appear as harmonics of the original disturbance appearing as a sequence of peaks, first at one half of the original scale, then one third, and so on until the flow becomes too complicated to discern individual peaks in the spectra. Although there are two shear layers in the distorted flow field, the vertical shear and the spanwise shear, it is the vertical shear layer that dominates the secondary instability process. It is stronger both in magnitude, and also in absolute velocity difference, both of which result in larger growth rates of an instability wave. The secondary instability is most clearly seen in the $v$-component, but we have also isolated it in the $w$-component. However, for the latter case, the symmetry constraints of the particular calculation, along with the effects of cross-flow instability mechanisms, cause the spatial distribution of the oscillations to be on either side of the centreline. The detection of the secondary instability is in contrast to recent numerical results of Henningson, Johansson & Lundbladh (1989) who did observe nonlinear effects due to wave–wave interactions, but not due to secondary instabilities. Their results were for plane Poiseuille flow and at a different Reynolds number. However, this discrepancy still needs to be resolved.

The central importance of the inclined shear layer in the growth of the disturbance is emphasized by the comparisons between the positive and the negative disturbances. In both cases, the nonlinear growth and the secondary instabilities are associated with the shear-layer structures, and in the case of the negative disturbance, it is the side lobes of the initial perturbation that provide these shear layers which subsequently act as 'nuclei' for the rapid nonlinear growth of the overall perturbation.

There is also a clear association between the structures observed in this study and the three-dimensional lambda vortices that have been observed in previous transition studies (for example, Klebanoff, Tidstrom & Sargent 1962). The shear layer and the secondary oscillations are both well known in the context of the three-dimensional development of boundary-layer transition but have always been viewed as a consequence of the breakdown of two-dimensional Tollmien–Schlichting waves. What has been shown here is that the T–S waves are not required, but that these localized structures are the natural consequence of any three-dimensional disturbance in a shear flow. Clearly, these ideas also have considerable relevance to Morkovin's (1969) work regarding the nonlinear 'bypass' mechanism by which a laminar flow can undergo transition to turbulence directly, bypassing the T–S wave-growth stage altogether.

The elongated low- and high-speed regions that develop as the disturbance progresses are also reminiscent of the high- and low-speed streaks that are observed in fully turbulent wall flows. This association is not just by chance. The work of Johansson, Alfredsson & Kim (1987) on the dynamics of the wall region of a turbulent flow suggests that the structures responsible for the majority of turbulence production are inclined shear layers whose structure is similar in many aspects to the shear-layer structures that we have discussed in this paper. In recent work, Landahl (1990) has shown that a theoretical model based on the interaction between the three-dimensional liftup of fluid elements and the background shear can explain the formation of the streaky structure that is commonly observed in wall-bounded

turbulent flows. These results reinforce the idea that transitional flows and turbulent flows have much in common and that the underlying dynamics may be the same. This has been discussed by Blackwelder (1983) and also, more recently by Breuer, Landahl & Spalart (1987), and by Breuer (1988).

The authors would like to thank Philippe Spalart for the use of his boundary-layer code and the NASA/Stanford Center for Turbulence Research where the simulations were performed. We also would like to thank Joe Haritonidis and Lawrence Gresko for their assistance and advice during the course of this work. This work was initiated at MIT with support from ONR Contract No. N00014-87-K-0048 and the ONR Graduate Fellowship Program and completed at the Center for Fluid Mechanics, Turbulence and Computation at Brown University, supported by DARPA-URI grant N00014-86-K0754.

## REFERENCES

BLACKWELDER, R. F. 1983 Analogies between transitional and turbulent boundary layers. *Phys. Fluids.* **26**, 2807–2815.

BREUER, K. S. 1988 The development of a localized disturbance in a boundary layer. PhD thesis, Massachusetts Institute of Technology, Department of Aeronautics and Astronautics, Cambridge, Mass.

BREUER, K. S. & HARITONIDIS, J. H. 1990 The evolution of a localized disturbance in a laminar boundary layer. Part 1. Weak disturbances. *J. Fluid Mech.* **220**, 569–594.

BREUER, K. S., LANDAHL, M. T. & SPALART, P. R. 1987 The simulation of coherent structures in a laminar boundary layer. In *Proc. 1987 Summer Program*, Stanford/NASA Center for Turbulence Research.

CASE, K. M. 1960 Stability of inviscid plane Couette flow. *Phys. Fluids.* **3**, 143–148.

GASTER, M. 1975 A theoretical model for the development of a wave packet in a laminar boundary layer. *Proc. R. Soc. Lond.* A **347**, 271–289.

GASTER, M. & GRANT, I. 1975 An experimental investigation of the formation and development of a wave packet in a laminar boundary layer. *Proc. R. Soc. Lond.* A **347**, 253–269.

GUSTAVSSON, L. H. 1978 On the evolution of disturbances in boundary layer flows. *Trita-Mek*-78-02. Department of Mechanics, Royal Institute of Technology, Stockholm.

HENNINGSON, D. S. 1988 The inviscid initial value problem for a piecewise linear mean flow. *Stud. Appl. Maths* **78**, 31–56.

HENNINGSON, D. S., JOHANSSON, A. V. & LUNDBLADH, A. 1989 On the evolution of localized disturbances in laminar shear flows. In *Proc. Third IUTAM Symposium on Laminar–Turbulent transition, Toulouse.* (To be published by Springer.)

HENNINGSON, D. S., SPALART, P. & KIM, J. 1987 Numerical simulations for turbulent spots in plane Poiseuille and boundary layer flows. *Phys. Fluids.* **30**, 2914–2917.

JOHANSSON, A. V., ALFREDSSON, P. H. & KIM, J. 1987 Shear layer structure in near wall turbulence. In *Proc. 1987 Summer Program*, pp. 237–251. NASA/Stanford Center for Turbulence Research.

JOHANSSON, A. V., HER, J. & HARITONIDIS, J. H. 1987 On the generation of high amplitude wall-pressure peaks in turbulent boundary layers and spots. *J. Fluid Mech.* **175**, 119–142.

KLEBANOFF, P. S., TIDSTROM, K. D. & SARGENT, L. M. 1962 The three-dimensional nature of boundary layer instability. *J. Fluid Mech.* **12**, 1–34.

KOVASZNAY, L. S. G., KOMODA, H. & VASUDEVA, B. R. 1962 Detailed flow field in transition. In *Proc. 1962 Heat Transfer and Fluid Mechanics Institute, Stanford University*, pp. 1–26.

LANDAHL, M. T. 1975 Wave breakdown and turbulence. *SIAM J. Appl. Maths* **28**, 735–756.

LANDAHL, M. T. 1980 A note on an algebraic instability of inviscid parallel shear flows. *J. Fluid Mech.* **98**, 243–251.

LANDAHL, M. T. 1990 On sublayer streaks. *J. Fluid Mech.* **212**, 593–614.

LANDAHL, M. T., BREUER, K. S. & HARITONIDIS, J. H. Dec. 1987 Transients and waves in boundary layer transition. In *Nonlinear Wave Interactions in Fluids*, pp. 17–21. Boston, MA: ASME.

MORKOVIN, M. V. 1969 The many faces of transition. In *Viscous Drag Reduction* (ed. C. Wells). Plenum.

ORSZAG, S. A. & PATERA, A. T. 1983 Secondary instability of wall-bounded shear flows. *J. Fluid Mech.* **128**, 347–385.

SPALART, P. R. 1986 Numerical simulation of boundary layers: Part 1. Weak formulation and numerical method. *NASA TM* 88222.

SPALART, P. R. 1988 Direct simulation of a turbulent boundary layer up to $Re_\theta = 1410$. *J. Fluid Mech.* **187**, 61–98.

SPALART, P. R. & YANG, K. 1987 Numerical study of ribbon induced transition in blasius flow. *J. Fluid Mech.* **178**, 345–365.

STUART, J. T. 1960 On the nonlinear mechanics of wave disturbances in stable and unstable parallel flows. I. The basic behavior in plane Poiseuille flow. *J. Fluid Mech.* **9**, 353.

STUART, J. T. 1965 The production of intense shear layers by vortex stretching and convection. *AGARD Rep.* 514.

SWEARINGEN, J. D. & BLACKWELDER, R. F. 1987 The growth and breakdown of streamwise vortices in the presence of a wall. *J. Fluid Mech.* **182**, 255–290.

WRAY, A. & HUSSAINI, M. Y. 1984 Numerical experiments in boundary layer stability. *Proc. R. Soc. Lond.* A **392**, 373–389.